Yu, H., and J.V. Cox. "An Analytical Study of the Radial Elastic Interaction between FRP Reinforcing Bars and Concrete," American Society for Composites' 15th Annual Technical Conference, Texas A&M University, September 2000, 8 pp.

An Analytical Study of the Radial Elastic Interaction between FRP Reinforcing Bars and Concrete

by Hailing Yu and James V. Cox

ABSTRACT

The surface structure of reinforcing elements within a matrix can produce a complex mechanical interaction including mechanical interlocking along the interface. The interlocking can be modeled using an interface idealization at a scale in which the details of the surface structure are omitted and the actual interface traction is homogenized over a length characteristic of the surface structure. For some applications such as the reinforcement of concrete with FRP bars, the reinforcing element can be idealized as being a circular cylinder, and the radial elastic interaction can affect the predicted bond behavior and failure mode. The radial elastic modulus for the interface of the "homogenized model" is defined by requiring static equivalence of the actual and homogenized tractions and equal amounts of strain energy in the domains. A unit cell approach is taken idealizing the traction distribution as periodic, and an analytical solution for the strain energy in the reinforcing element is presented. The analytical expression for the elastic modulus reflects its dependence upon the traction distribution, material properties, and bar geometry. To study the effects of these parameters, the bond specimen of an FRP bar in a concrete matrix is examined. As the actual traction distribution becomes more concentrated, the interface of the homogenized model becomes more compliant. For the current example of an FRP bar in normal strength concrete, the radial elastic modulus is most sensitive to changes in the transverse Young's modulus of the FRP bar. The elastic modulus is applied to accurately reproduce the effects of a nonuniform traction distribution even when the concrete fails due to longitudinal cracking and snap-back behavior occurs in the radial response. The traction distribution and compliance of the FRP bar have a significant effect on the snap-back behavior indicating the potential for a very sudden failure due to concrete cracking.

INTRODUCTION

Interface descriptions of the mechanical interaction between two constituent materials of a body are common in computational mechanics. The characterization of this interaction often includes an elastic component with different interpretations depending upon the application [1]. In this study, the elastic component is defined to characterize the local elastic response associated with mechanical interlocking between *surface structures* (i.e., the deviation of the actual geometry from that of an idealized model such as a circular cylinder), which are not explicitly modeled at a larger scale.

Recently Cox and Yu [1] derived an analytical expression for the elastic modulus of an interface model characterizing the elastic interaction between a slender axisymmetric reinforcing element and a matrix. The study [1] was motivated by the need for computational models at a scale in which the reinforcement and matrix are

modeled as solids, and an interface model is used to characterize the progressive failure of the mechanical interaction.

The current research (see [2] for more details) differs from the earlier study [1] in the motivating problem. In the previous study, the deformation of the reinforcement was neglected, thus the formulation was limited to composites with reinforcing elements (e.g., steel) having a small transverse compliance relative to the matrix (e.g., concrete). In this study, the motivating problem is the mechanical interaction between fiber-reinforced polymer (FRP) reinforcing bars and a concrete matrix. For FRP bars the transverse compliance is approximately 20 to 30 times that of steel and approximately 2 to 4 times that of concrete, thus the local deformation of both the matrix and reinforcement are now considered. The increased radial compliance of the FRP bars affects the mechanical interlocking. For example, "cyclic bond stress vs. slip behavior" has been observed for several bond tests of FRP bars (see e.g., [3,4]). The spatial period of the response cycles corresponds to the length of the periodic surface structure of the bar, reflecting that there must be significant radial compliance.

Similar to steel bars, many FRP bars have a fabricated surface structure that produces a significant mechanical interlocking with the adjacent concrete. The mechanical interlocking produces a complicated interface traction distribution due to the resulting contact conditions. The radial component of the traction tends to produce significant hoop stress in the adjacent concrete and can fail the concrete in longitudinal cracking[1] (see e.g., Tepfers [5]). One motivation for examining the radial compliance is that it can significantly affect the bond strength and failure mode for an FRP bar in a concrete matrix (pull-out *vs*. failure due to longitudinal cracking – *splitting failure*). For computational "bond models" in which the surface structure geometry is explicitly modeled (*rib-scale* models [6]) the detailed effects of the mechanical interlocking are accounted for directly. A larger scale of modeling (*bar scale* [6]) amenable to the analysis of structural components represents the reinforcement as an cylindrical solid (eliminating the geometric detail of the surface structure) and uses an interface idealization to characterize the effects of mechanical interlocking. This type of model was recently used by Guo and Cox [7,8] to reproduce the behavior of various test specimens. The model represents the kinematics of the mechanical interlocking (i.e., the "wedging effect" of the surface structure) through an inelastic radial dilation of the interface which is partially negated by an elastic radial contraction of the interface. Unfortunately while the tangent elastic response can be estimated from experimental data, experimental data on the radial elastic response is not available. Thus further investigation of the radial elastic modulus associated with the interface is needed.

This paper focuses on the radial elastic response attributed to an interface idealization when the actual traction distribution along the interface is assumed to be axisymmetric and nonuniform (but periodic) in the axial direction. The paper is organized into sections that address the following areas: (2) idealizations of analytical models needed to define the elastic modulus of the interface, (3) brief review of analytical solution, (4) use of the analytical solution to determine an equivalent elastic modulus of the interface idealization and parameter studies, (5) application of the model in predicting longitudinal cracking in a concrete matrix, and (6) summary and conclusions. Additional details are available in reference [2].

[1] Ideal longitudinal cracks occur in a θ-plane assuming a cylindrical coordinate system in which the z-axis is aligned with the axis of the bar.

ANALYTICAL MODEL

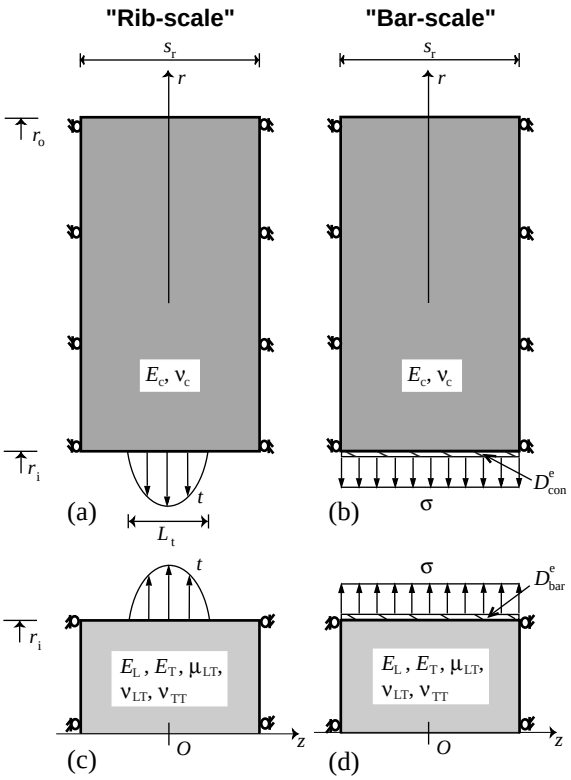

Figure 1. Idealized analytical models.

To define an elastic modulus for an interface idealization that incorporates analytical solutions, a few simplifications are adopted at both scales (rib-scale and bar-scale). At both scales the interface is idealized as being smooth. At the smaller scale (rib-scale), the effect of mechanical interlocking is represented by a more concentrated interfacial traction distribution. For the bar-scale model the actual traction is homogenized over a characteristic length, e.g., the length of spatial periodicity of the surface structure. By definition, the actual and homogenized tractions are statically equivalent loads, but their mechanical effects differ.

Figures 1(a-d) show θ-sections of the axisymmetric rib- and bar-scale models. The concrete is modeled as a thick-walled cylinder and idealized as being homogeneous, isotropic and linear elastic (Young's modulus E_c and Poisson's ratio ν_c). The FRP cylinder is treated as transversely isotropic and linear elastic with five independent material constants: longitudinal Young's modulus (E_L), transverse Young's modulus (E_T) and Poisson's ratio (ν_{TT}), and longitudinal-transverse shear modulus (μ_{LT}) and Poisson's ratio (ν_{LT}).

Let s_r denote the characteristic length associated with the assumed periodic structure (e.g., rib-spacing) along the longitudinal axis (z-axis). In Figures 1(a-d) the elastic problems are defined for a unit cell of length s_r. The rollers along the edges $z=\pm s_r/2$ and the radial traction distributions (even about the r-axis) produce response symmetries consistent with the unit cell assumptions. For the rib-scale model (Figures 1a,c) the radial traction distribution t is nonzero over the contact length L_t, and for the bar-scale model (Figures 1b,d) σ denotes the homogenized traction over s_r. The tractions are related through static equivalence as

$$\sigma = \frac{1}{s_r}\int_{-s_r/2}^{s_r/2} t(z)dz \tag{1}$$

The interface model for the bar-scale problem has a *radial elastic stiffness* (denoted as D^e) that relates σ to the relative radial displacement (δ_n) of initially coincident points on the interface (positive in extension). The radial elastic stiffness of the interface (for brevity, the *interface stiffness*) has dimensions of force per length^3. Alternatively, deformations of the interface are often nondimensionalized by characteristic lengths that can be related to the surface structure (see e.g., [6,9]); thus some results will be presented in terms of a generalized strain measure defined as

$$q_n=\delta_n/d_b \tag{2}$$

where $d_b=2r_i$, the bar diameter. (The surface structure scales with d_b for typical FRP bars.) The corresponding *radial elastic modulus* relating σ and q_n is denoted

by $\hat{D}^{\mathrm{e}}$. Thus σ is related to the interface stiffness, elastic modulus and kinematic variables by

$$\sigma = D^{\mathrm{e}}\delta_{\mathrm{n}} = \hat{D}^{\mathrm{e}} q_{\mathrm{n}} \qquad D^{\mathrm{e}} = \hat{D}^{\mathrm{e}}/d_{\mathrm{b}} \tag{3a,b}$$

The increase in compliance associated with the concentration of the actual interface traction can be additively decomposed into parts associated with the concrete ($1/D^{\mathrm{e}}_{\mathrm{con}}$, Figure 1b) and reinforcing bar ($1/D^{\mathrm{e}}_{\mathrm{bar}}$, Figure 1d); i.e., the interface compliance satisfies

$$D^{\mathrm{e}\,-1} = D^{\mathrm{e}\ -1}_{\mathrm{con}} + D^{\mathrm{e}\ -1}_{\mathrm{bar}} \qquad \hat{D}^{\mathrm{e}\,-1} = \hat{D}^{\mathrm{e}\ -1}_{\mathrm{con}} + \hat{D}^{\mathrm{e}\ -1}_{\mathrm{bar}} \tag{4a,b}$$

By Equation (1) the rib- and bar-scale models are equivalent in the Saint-Venant sense. Further, we equate the strain energies stored in the elastic bodies of problems (a,c) to those of problems (b,d). We select this equivalence measure because potentially the strain energy can be released to drive cracks in the materials. Since the strain energy stored in an elastic body is equal to the work done by external loading, the "energy equivalence" requires

$$W^{t}_{\mathrm{a}} = W^{\sigma}_{\mathrm{b}} \qquad W^{t}_{\mathrm{c}} = W^{\sigma}_{\mathrm{d}} \tag{5a,b}$$

where W^{t}_{a} denotes the work done by t in problem (a), and so on. Solving expressions for the elastic modulus from Equations (4) and (5) requires that each work expression be obtained analytically. The next section gives a brief overview of the procedure for solving these elasticity problems.

ANALYTICAL SOLUTION

The solution approach for problem (c) is the same as that previously used for problem (a) [1], where the variations of the displacements in the z-direction are expressed in terms of orthonormal trigonometric bases (i.e., a Fourier series approach). The bases for even and odd functions of z are

$$\Phi_{cn}(z) = \begin{cases} \dfrac{1}{\sqrt{s_{\mathrm{r}}}}, & n = 0 \\ \dfrac{\cos(z\omega_n)}{\sqrt{s_{\mathrm{r}}/2}}, & n > 0 \end{cases}, \qquad \Phi_{sn}(z) = \frac{\sin(z\omega_n)}{\sqrt{s_{\mathrm{r}}/2}}, \qquad \omega_n = \frac{2\pi n}{s_{\mathrm{r}}}. \tag{6a-c}$$

Due to the symmetry of the problem, the nonzero displacements u_r and u_z are even and odd functions of z, respectively, and thus can be expressed as

$$u_r(r,z) = \sum_{n=0}^{\infty} v_{rn}(r)\Phi_{cn}(z), \qquad u_z(r,z) = \sum_{n=1}^{\infty} v_{zn}(r)\Phi_{sn}(z). \tag{7a,b}$$

Substituting the above definitions into the strain-displacement and constitutive relationships yields the stress components as

$$\sigma_{rr}(r,z) = \sum_{n=0}^{\infty} \sigma_n(r)\Phi_{cn}(z), \qquad \sigma_{rz}(r,z) = \sum_{n=1}^{\infty} \tau_n(r)\Phi_{sn}(z), \tag{8a,b}$$

The coefficient functions are projections of the solutions onto the basis, e.g.,

$$v_{rn}(r) = \langle u_r(r,z), \Phi_{cn}(z)\rangle, \qquad v_{zn}(r) = \langle u_z(r,z), \Phi_{sn}(z)\rangle \tag{9a,b}$$

The solutions to the coefficient functions can be obtained by substituting the series expressions into the governing equations, solving the resulted differential equations, and applying the traction boundary conditions for the unknown constants

$$\sigma_{rr}\big|_{r=r_{\mathrm{i}}} = t, \qquad \sigma_{rz}\big|_{r=r_{\mathrm{i}}} = 0, \tag{10a,b}$$

where t denotes a generic distribution of traction normal to the surface (Figure 1c). The traction t can also be projected onto the basis

$$\left\langle \Phi_{cn}, \sigma_{rr} \right\rangle\Big|_{r=r_\mathrm{i}} = \left\langle \Phi_{cn}, t \right\rangle = \alpha_n \qquad \text{(11a,b)}$$

where the α's are the coordinates of t in the Φ_c basis (i.e., Fourier coefficients of t). Details of the solution procedure are presented in [2] and are omitted here for brevity.

ELASTIC MODULUS

The work done by t in problem c (Figure 1c) can be calculated as follows

$$W_\mathrm{c}^t = \int_{-s_\mathrm{r}/2}^{s_\mathrm{r}/2} \tfrac{1}{2}\left[2\pi r_\mathrm{i} t(z)\right] u_r^{\mathrm{bar}}(r_\mathrm{i}, z)\, dz = \pi r_\mathrm{i} \sum_{n=0}^{\infty} \alpha_n v_{rn}^{\mathrm{bar}}(r_\mathrm{i}) = W_0^{\mathrm{bar}} + \pi r_\mathrm{i} \sum_{n=1}^{\infty} \alpha_n v_{rn}^{\mathrm{bar}}(r_\mathrm{i}) \qquad \text{(12a)}$$

where the superscript "bar" denotes the bar subdomain, α_n and $v_{rn}(r_\mathrm{i})$ are the Fourier coefficients of t and $u_r(r_\mathrm{i},z)$, respectively, and $W_0=\pi r_\mathrm{i}\alpha_0 v_{r0}(r_\mathrm{i})$ is the work done by a uniformly distributed radial traction σ acting over a surface of length s_r. In a similar manner, applying the elastic solution for the concrete subdomain [1] and the definitions of Equations (2,3a), we can explicitly write the other work terms of Equations (5) as

$$W_\mathrm{a}^t = W_0^{\mathrm{con}} - \pi r_\mathrm{i} \sum_{n=1}^{\infty} \alpha_n v_{rn}^{\mathrm{con}}(r_\mathrm{i}) \qquad \text{(12b)}$$

$$W_\mathrm{b}^\sigma = W_0^{\mathrm{con}} + \pi r_\mathrm{i} s_\mathrm{r} \sigma^2 d_\mathrm{b} \big/ \hat{D}_{\mathrm{con}}^{\mathrm{e}}, \qquad W_\mathrm{d}^\sigma = W_0^{\mathrm{bar}} + \pi r_\mathrm{i} s_\mathrm{r} \sigma^2 d_\mathrm{b} \big/ \hat{D}_{\mathrm{bar}}^{\mathrm{e}} \qquad \text{(12c,d)}$$

where $d_\mathrm{b}=2r_\mathrm{i}$ and the superscript "con" denotes concrete. Substituting Equations (12a-d) into Equations (4b) and (5) and solving for $\hat{D}^{\mathrm{e}}$ gives

$$\hat{D}^{\mathrm{e}} = s_\mathrm{r}\sigma^2 d_\mathrm{b} \left\{ \sum_{n=1}^{\infty} \alpha_n \left[-v_{rn}^{\mathrm{con}}(r_\mathrm{i}) + v_{rn}^{\mathrm{bar}}(r_\mathrm{i}) \right] \right\}^{-1} \qquad \text{(13)}$$

Cox and Yu [1] gave $\hat{D}_{\mathrm{con}}^{\mathrm{e}}$ for the case of "r_o sufficiently large relative to r_i" (e.g. $r_\mathrm{o}/r_\mathrm{i}\geq 2$) as follows

$$\hat{D}_{\mathrm{con}}^{\mathrm{e}} = \left(\sum_{n=1}^{\infty} -\frac{\alpha_n^2 \kappa_n}{\alpha_0^2 E_\mathrm{c}} \right)^{-1} \qquad \text{(14)}$$

where κ_n is nondimensional and given by

$$\kappa_n = \left(1-\nu_\mathrm{c}^2\right) K_1^2(\omega_n r_\mathrm{i}) \Big/ \left\{ (\omega_n r_\mathrm{i})^2 \left[K_0^2(\omega_n r_\mathrm{i}) - K_1^2(\omega_n r_\mathrm{i}) \right] - 2\left(1-\nu_\mathrm{c}\right) K_1^2(\omega_n r_\mathrm{i}) \right\} \qquad \text{(15)}$$

$K \sim$ modified Bessel functions of the second kind.

The radial elastic modulus for the interface of an FRP bar is

$$\hat{D}_{\mathrm{bar}}^{\mathrm{e}} = \left(\sum_{n=1}^{\infty} \frac{\alpha_n^2 \xi_n}{\alpha_0^2 B_n} \right)^{-1} \qquad \text{(16)}$$

where ξ_n is dimensionless and given by

$$\xi_n = \tfrac{1}{2}\left(p\eta_q - q\eta_p\right) I_1(p\omega_n r_\mathrm{i}) I_1(q\omega_n r_\mathrm{i}) \qquad \text{(17)}$$

$I \sim$ modified Bessel functions of the first kind, and

$$\begin{aligned} B_n = {} & \omega_n r_\mathrm{i}(-\eta_p + p)(C_{13} + C_{11} q \eta_q) I_0(q\omega_n r_\mathrm{i}) I_1(p\omega_n r_\mathrm{i}) + \\ & \omega_n r_\mathrm{i}(\eta_q - q)(C_{13} + C_{11} p \eta_p) I_0(p\omega_n r_\mathrm{i}) I_1(q\omega_n r_\mathrm{i}) + \\ & (q\eta_p - p\eta_q)(C_{11} - C_{12}) I_1(p\omega_n r_\mathrm{i}) I_1(q\omega_n r_\mathrm{i}) \end{aligned} \qquad \text{(18)}$$

has units of Young's modulus [2]. The radial elastic modulus accounting for both contributions can be written as

TABLE I. SPECIMEN DATA.

E_L (GPa)	E_T (GPa)	μ_{LT} (GPa)	ν_{LT}	ν_{TT}	E_c (GPa)	ν_c
39.8	9.29	3.78	0.274	0.42	30.7	0.17

L_t (mm)	r_i (mm)	s_r (mm)	L_t/s_r	r_i/s_r	r_o/r_i
4.29	9.525	34.3	0.125	0.28	4.0

$$\hat{D}^e = \left(\hat{D}_{con}^{e\ -1} + \hat{D}_{bar}^{e\ -1}\right)^{-1} = \left[\sum_{n=1}^{\infty} \frac{\alpha_n^2}{\alpha_0^2}\left(\frac{\xi_n}{B_n} - \frac{\kappa_n}{E_c}\right)\right]^{-1} \tag{19}$$

The above analytical results will now be applied to the bond specimen of Malvar [10] using the "type D" GFRP bar (Table I). The bar has a helical surface, and a relatively concentrated interface contact (L_t/s_r=1/8) is assumed. Such concentrated contact is possible since the surface misfit between the bar and concrete can be significant when relative slip occurs. The concrete used in the specimen has normal strength. The ratio r_o/r_i verifies the assumption that the hollow cylinder of concrete is "sufficiently thick" for the previous solution [1] to be applicable. $\hat{D}^e$ is dependent on the traction distribution (via α_n/α_0), the seven independent material constants of the FRP and concrete and r_i/s_r (via $\omega_n r_i$). Parameter studies addressing the first two factors are presented in the next three sub-sections.

Effect of Traction Distribution

We consider three types of traction distributions: uniform, half-cosine and triangular [2]. The traction distribution affects the radial elastic modulus of the interface via the term α_n/α_0. The "nondimensionalized contact length" (β=L_t/s_r) and the distribution type affect the concentration of the traction. For the same distribution type, the traction is more concentrated for a smaller β; whereas for the same value of β, the traction is most concentrated for the triangular distribution and least for the uniform distribution.

The effect of the traction distribution is examined in Figure 2. $\hat{D}^e/E_c$ *vs*. L_t/s_r (β) is plotted for the three types of distributions. An increased concentration of the traction (either due to distribution type or β) produces a more compliant interface. As β decreases the effect of the distribution type upon the elastic modulus decreases (e.g., the two non-uniform distributions give very close predictions for a large range of β). For full-contact (β=1) the elastic modulus becomes infinite for the uniform traction case (since the traction distributions of the rib-scale and bar-scale models are the same), but finite for any other traction distribution representing full-contact.

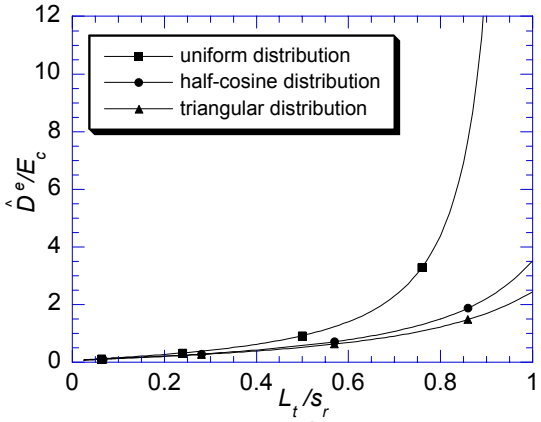

Figure 2. Dependence of $\hat{D}^e$ on contact length and traction distribution type.

Effect of Material Constants

Figure 3 contains the results of a parameter study on the effects that the seven independent material constants have on $\hat{D}^e$. Percent changes in $\hat{D}^e$ *vs*. percent changes in each material constant are shown. A half-cosine distribution of traction and β=1/8 (Table I) were assumed in the calculations. Changes in E_L, ν_{LT} and ν_c have the least effects on $\hat{D}^e$. For the current example, changes in E_c, ν_{TT} and μ_{LT} do not have the largest effects but do produce relatively significant changes, whereas changes in E_T have the most significant effect on $\hat{D}^e$.

Effect of Bar Geometry

The parameter r_i/s_r (bar radius / rib spacing) affects $\hat{D}^e$ through the argument of the modified Bessel functions. Parameter studies [2] have shown that the elastic modulus decreases as r_i/s_r decreases; however, the variation in the FRP contribution becomes very small when r_i/s_r is relatively small. The effect of the FRP on the elastic compliance is greater than that of the concrete, but the difference in the two contributions decreases with r_i/s_r.

APPLICATION

The mechanical interaction between FRP bars and concrete provides a good application area for the developed theory. We examine the bond specimen described in Table I and adopt axisymmetric finite element models. The FRP is idealized as being transversely isotropic and linear elastic. The concrete is modeled as quasibrittle, with three longitudinal cracks modeled as *cohesive cracks* [2]. Axisymmetric FE models of the unit cell of the bond specimen were developed at both scales – the rib- and bar-scales (Figure 1). The case of a uniformly distributed t over L_t is examined, thus the rib-scale model is referred to as being "ring-loaded." The "bar-scale" or homogenized model incorporates a homogenized traction and an interface with a stiffness D^e defined by Equations (3b) and (19).

The "interface responses" of the two types of models are compared in Figure 4. The magnitude of σ (t L_t/s_r for the ring-loaded models) *vs*. Δu (relative displacement) is compared for each of the constituent materials and their combination. Figure 5 examines the response for contact ratios (L_t/s_r) of: 1, 1/2, 1/4, and 1/8. The main observations are:

1. The responses of both types of models are nearly indistinguishable for the concrete, FRP and their combination.
2. The specimen exhibited snap-back behavior in the radial response. The added

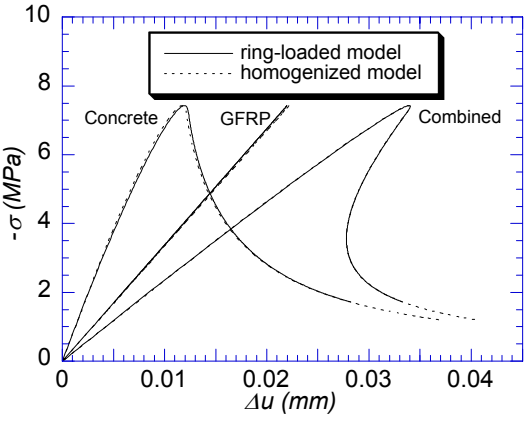

Figure 4. Radial compression vs. interface separation.

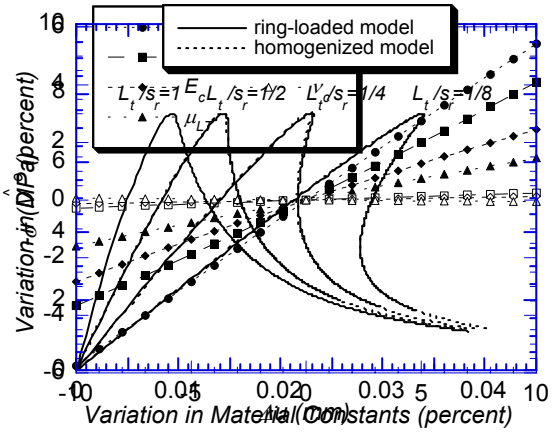

Figure 5. Parameter studies of elastic constants.

Figure 5. Radial compression vs. interface separation under different contact conditions.

compliance of the FRP increases the amount of elastic strain energy stored at the peak load and the potential of snap-back behavior in the radial response.
3. The potential for snap-back behavior increases with a reduction in the contact area because of the increased elastic energy stored in local deformation.

SUMMARY AND CONCLUSIONS

By accounting for "static equivalence" and "energy equivalence" the radial elastic response due to a known traction distribution along an interface (e.g., attributed to mechanical interlocking) can be accurately represented in a larger scale (i.e., homogenized) model. The actual traction distribution causes deformation of each constituent material which can be represented by additional interface compliance in the homogenized model. By making several simplifying assumptions and adopting a unit cell approach, expressions for the radial elastic modulus can be obtained in closed form. The theoretical development of the radial elastic modulus is applicable to the problem of the mechanical interaction between FRP bars and concrete. A bond specimen is examined to study the effects of traction distribution, material properties, and bar geometry on the radial elastic modulus. Among the findings were:

1. An increased concentration of the actual traction (either due to distribution type or contact length) produces a more compliant interface in the homogenized model.
2. Changes in E_L, ν_{LT} and ν_c have negligible effects on the variation of $\hat{D}^e$, whereas D^e is most sensitive to changes in E_T for normal strength concrete.
3. Reducing r_i/s_r leads to a decreased elastic modulus.

The same bond specimen was used to examine how $\hat{D}^e$ may affect the radial response when the concrete develops longitudinal cracking by comparing the homogenized model (bar-scale) to a rib-scale model. Among the findings were:

1. The responses of both types of models are nearly indistinguishable.
2. Snap-back behavior occurred in part due to the elastic energy associated with local deformation. Both the relative compliance of the two constituent materials and the contact condition have a significant effect upon the snap back behavior.

ACKNOWLEDGMENTS

Support for this study by the National Science Foundation (grant no. CMS-9872609), Naval Facilities Engineering Service Center (contract no. N0024499P2444), and the Office of Naval Research is gratefully acknowledged.

REFERENCES

1. Cox, J.V. and H. Yu. 1999. "A Micromechanical Analysis of the Radial Elastic Response associated with Slender Reinforcing Elements within a Matrix," *Journal of Composite Materials*, 33(23):2161-2192.
2. Yu, H. and J.V. Cox. 1999. "Radial Elastic Modulus for the Interface between FRP Reinforcing Bars and Concrete," *Journal of Reinforced Plastics and Composites*, in press.
3. Cox, J.V., K. Bergeron, and L.J. Malvar. 2000. "A Combined Experimental and Analytical Study of the Bond between Lightweight Concrete and CFRP Bars," presented at ASCE's 14th Engineering Mechanics Division Conference, Austin, Texas.
4. Benmokrane, B., B. Tighiouart, and O. Chaallal. 1996. "Bond Strength and Load Distribution of Composite GFRP Reinforcing Bars in Concrete," *ACI Materials Journal*, 93(3):246-253.
5. Tepfers, R. 1979. "Cracking of Concrete Cover along Anchored Deformed Reinforcing Bars," *Magazine of Concrete Research*, 31(106):3-12.

6. Cox, J.V. and L.R. Herrmann. 1998. “Development of A Plasticity Bond Model for Reinforced Concrete,” *Mechanics of Cohesive-frictional Materials*, John Wiley and Sons, 3:155-180.
7. Guo, J. and J.V. Cox. 2000. “An Interface Model for the Mechanical Interaction between FRP Bars and Concrete,” *Journal of Reinforced Plastics and Composites*, 19(1):15-33.
8. Cox, J.V. and J. Guo. 1999. “Modeling the Stress State Dependency of the Bond Behavior of FRP Tendons,” ACI Special Publication, *Fourth International Symposium on FRP Reinforcement for RC Structures*, Baltimore, Maryland.
9. Needleman, A. 1992. “Micromechanical Modeling of Interfacial Decohesion,” *Ultrmicroscopy*, 40:203-214.
10. Malvar, L.J. 1995. “Tensile and Bond Properties of GFRP Reinforcing Bars,” *ACI Materials Journal*, 92(3):276-285.